Tuning Ion Transport and Selectivity by a Salt Gradient in a Charged Nanopore

ARTICLE *in* ANALYTICAL CHEMISTRY · JANUARY 2014

Impact Factor: 5.64 · DOI: 10.1021/ac4040136 · Source: PubMed

4 AUTHORS, INCLUDING:

Li-Hsien Yeh
National Yunlin University of Science and Tec…
63 PUBLICATIONS **717** CITATIONS
SEE PROFILE

Chris Hughes
University of Central Florida
3 PUBLICATIONS **30** CITATIONS
SEE PROFILE

Shizhi Qian
Old Dominion University
156 PUBLICATIONS **2,513** CITATIONS
SEE PROFILE

analytical chemistry

Article

pubs.acs.org/ac

Tuning Ion Transport and Selectivity by a Salt Gradient in a Charged Nanopore

Li-Hsien Yeh,*[,†,∥] Christopher Hughes,[‡,∥] Zhenping Zeng,[§] and Shizhi Qian*[,‡]

[†]Department of Chemical and Materials Engineering, National Yunlin University of Science and Technology, Yunlin 64002, Taiwan
[‡]Department of Mechanical and Aerospace Engineering, Old Dominion University, Norfolk, VA 23529, United States
[§]School of Electronic and Optical Engineering, Nanjing University of Science and Technology, Nanjing 210094, P. R. China

ABSTRACT: Inspired by ion channels in biological cells where the intracellular and extracellular ionic concentrations are typically different, a salt concentration gradient through a charged nanopore is proposed to actively regulate its ion transport and selectivity. Results obtained show that, in addition to the ion current rectification phenomenon, a reversed ion selectivity of the nanopore occurs when the concentration gradient is sufficiently large. In addition, if the directions of the applied concentration gradient and electric field are identical, a reversed magnified electric field occurs near the cathode side of the nanopore. This induced field can be used to enhance the capture rate of biomolecules and is therefore capable of improving the performance of single biomolecule sensing using nanopores.

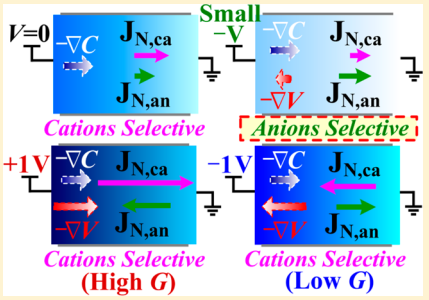

With growing interest in constructing nanofluidic devices for detection of single unlabeled biomolecules[1−4] and a fundamental understanding of how biological ion channels function,[5−7] ion transport in synthetic nanopores has recently received significant attention. When the nanopore's size is comparable to the electric double layer (EDL) thickness, several unique features, such as ion selectivity[7−11] and ion concentration polarization (ICP),[12−15] have been observed. Typical results showed that such ion selectivity resulting from fixed charges on the nanopore wall favors passage of counterions (i.e., larger contribution of the ionic current from counterions) and obstructs co-ions (i.e., smaller contribution of the ionic current from co-ions) through it.[10] In particular, the ion current rectification (ICR),[16−23] arising from asymmetric transport of cations and anions through the nanopore due to the EDL overlapping, would occur when the symmetric distributions of cations and anions on the nanopore are broken.[24] ICR exhibits a voltage bias polarity-dependent ion accumulation and depletion behavior in the nanopore and, therefore, an asymmetric current−voltage (I−V) diodelike behavior, implying that ions favorably move in one direction of the nanopore and are inhibited in the opposite direction. As a consequence, a thorough understanding of these ion transport phenomena in nanopores is crucial to provide new insight into the operation of biological ion channels and for the development of next-generation nanofluidic devices.

In living cells, an ion concentration gradient between the exterior and interior of the cell membrane is not only of fundamental significance to the transmembrane potential and ionic current,[25] but it also controls the function of ion channels and rectifies ionic species transporting through the cell.[5,7,26] Inspired by this, we investigated the electrokinetic ion transport in a short charged nanopore under a salt concentration gradient. Our results show that the ion transport and selectivity of a nanopore can be actively tuned by modulating the voltage bias and concentration gradients applied across the nanopore. As illustrated in Figure 1, we demonstrate, for the first time, that a reversed ion selectivity of the nanopore (i.e., the ionic current contributed from co-ions is larger than that of counterions) can be found, depending upon both the voltage bias polarities and the concentration gradients.

THEORETICAL MODEL

The problem under consideration is depicted in Figure 1a, where a solid-state membrane containing a cylindrical nanopore of length L_N and radius R_N separates two large, identical reservoirs of axial length L_r and radius R_r on either side. We assume both the nanopore and the reservoirs are filled with an incompressible, Newtonian fluid containing binary electrolytes (e.g., KCl). C_L and C_R denote the bulk electrolyte solution concentrations in the left and right reservoirs, respectively. An external potential bias, V, is applied between the two reservoirs to generate an ionic current through the nanopore. As illustrated in Figure 1b, we assume $C_L \geq C_R$, establishing a concentration gradient to regulate the ion transport and selectivity in the nanopore. Because of the axial symmetry of the present problem, a cylindrical coordinate system (r, z) is adopted with the origin located at the center of the nanopore.

The following verified continuum-based model,[10,11,13,27] comprising highly coupled Poisson-Nernst−Planck (PNP) equations and Stokes equations, is employed to describe the electrostatics, hydrodynamics, and ionic mass transport processes:

Received: December 11, 2013
Accepted: January 31, 2014
Published: January 31, 2014

dx.doi.org/10.1021/ac4040136 | Anal. Chem. 2014, 86, 2681−2686

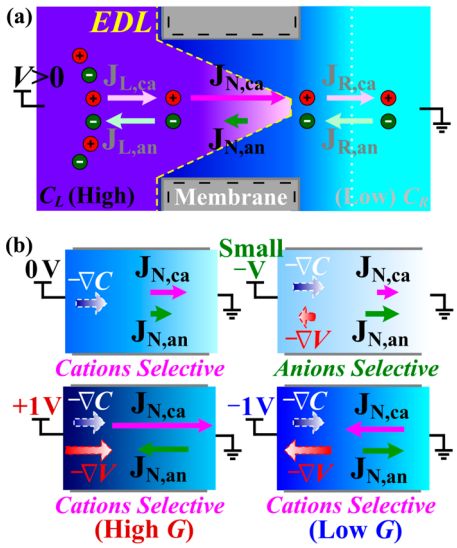

Figure 1. (a) Ion transport in a negatively charged solid-state nanopore under an applied salt concentration gradient. C_L and C_R denote the bulk salt concentrations in the left and right reservoirs, respectively. The right reservoir is grounded, and a potential bias, V, is applied at the left reservoir. The ionic fluxes, $\mathbf{J}$, at the left and right reservoirs and inside the nanopore are subscripted as L, R, and N, respectively. The subscripts "ca" and "an" denote the ionic fluxes, $\mathbf{J}$, of cations and anions, respectively. (b) Schematics showing how to tune the ion transport and selectivity using a concentration gradient across a negatively charged nanopore. $-\nabla C$ and $-\nabla V$ represent the driving forces arising from an applied concentration gradient and electric field, respectively.

$$-\varepsilon_f \nabla^2 \phi = \rho_e \tag{1}$$

$$\nabla\cdot\mathbf{J}_j = \nabla\cdot\left(\mathbf{u}c_j - D_j\nabla c_j - z_j\frac{D_j}{RT}Fc_j\nabla\phi\right) = 0,$$

$$j = 1 \text{ and } 2 \tag{2}$$

$$-\nabla p + \mu\nabla^2\mathbf{u} - \rho_e\nabla\phi = \mathbf{0} \tag{3}$$

$$\nabla\cdot\mathbf{u} = 0 \tag{4}$$

In the above, ϕ is the electric potential; $\rho_e = F\sum_{j=1}^{2} z_j c_j$ is the space charge density of mobile ions, and $\mathbf{J}_j$, c_j, D_j, and z_j are the ionic flux, concentration, diffusivity, and valence of the j^{th} ionic species, respectively ($j = 1$ for cations and $j = 2$ for anions). F, R, and T are the Faraday constant, universal gas constant, and absolute fluid temperature, respectively; ε_f, p, and μ are the permittivity, pressure, and viscosity of the fluid, respectively, and $\mathbf{u} = u\mathbf{e}_r + v\mathbf{e}_z$ is the fluid velocity with $\mathbf{e}_r$ and $\mathbf{e}_z$ being the unit vectors in the r and z directions, respectively. The first, second, and third terms in $\mathbf{J}_j$ denote the contributions from the convective, diffusive, and migrative fluxes, respectively. Note that, for $R_N \geq 3$ nm, the continuum-based models have been validated to be capable of capturing the essential physics of the transport of ions, fluid, and nanoparticles through a nanopore.[11,13,20,28−32] Corry et al.[33] also showed that, for $R_N > 1$ nm, the results based on the present PNP model agree well with those on Brownian dynamic simulation.

The following boundary conditions are assumed for eqs 1−4. (i) The ionic concentrations at the end of the left (right) reservoir reach their bulk values, $c_j = C_L$ ($c_j = C_R$), and the corresponding electric potentials are ϕ (left) = V and ϕ (right) = 0. (ii) The membrane wall is nonslip, ion-impenetrable, and bears a fixed surface charge density, σ_m, yielding $\mathbf{u} = \mathbf{0}$, $\mathbf{n}\cdot\mathbf{J}_j = 0$ and $-\mathbf{n}\cdot\nabla\phi = \sigma_m/\varepsilon_f$, respectively. Here $\mathbf{n}$ is the unit outer normal vector. Note that the effect of charge regulation on the membrane wall[34] is neglected in the present study. (iii) Slip boundary condition for the flow field, insulation boundary condition for the potential ($-\mathbf{n}\cdot\nabla\phi = 0$), and zero normal ionic fluxes ($\mathbf{n}\cdot\mathbf{J}_j = 0$) are imposed on the side boundaries of the two reservoirs, which are far away from the nanopore. (iv) A normal flow without an external pressure gradient ($p = 0$) is specified on both ends of the reservoirs. (v) Symmetric boundary condition is specified along the axis of the nanopore.

The conductance and selectivity of the nanopore, G and S, respectively, can be evaluated by[10,11]

$$G = I/V = [\int_\Lambda (\sum_{j=1}^{2} Fz_j\mathbf{J}_j)\cdot\mathbf{n}d\Lambda]/V \tag{5}$$

and

$$S = \frac{|I_{counter}| - |I_{co}|}{|I_{counter}| + |I_{co}|} \tag{6}$$

In the above, Λ denotes either end of the reservoirs. For a negatively charged nanopore filled with an aqueous KCl solution, the current contributed by counterions (i.e., K^+ ions) is $I_{counter} = F\int_\Lambda(\mathbf{J}_1\cdot\mathbf{n})\,d\Lambda$, while the current carried by Cl^- co-ions is $I_{co} = -F\int_\Lambda(\mathbf{J}_2\cdot\mathbf{n})\,d\Lambda$. In general, $S = 1$ (−1) and 0 denote a completely cation-selective (anion-selective) and nonselective nanopore, respectively.

The model is solved numerically by a commercial finite element package, COMSOL Multiphysics (version 3.5a, www.comsol.com), operated in a high-performance cluster. Similar systems related to electrokinetic ion[10,11,20,35] and nanoparticle[32,36−38] transport in charged nanopores have been successfully solved. The applicability of the model was also verified previously,[13,28] by comparing the predicted conductance[13] and ionic current change due to the translocation of DNA[28] through a silica nanopore with the experimental data obtained by Smeets et al.[39] A more detailed description of the numerical implementation is available in the literature.[40]

RESULTS AND DISCUSSION

For illustration, we consider a solid-state nanopore with dimensions (R_N = 10 nm and L_N = 60 nm) and the fixed surface charge density $\sigma_m = -60$ mC/m^2. The former is in accordance with the dimensions of nanopores drilled in silica membranes,[39,41] and the latter corresponds to the typical value for a silica nanopore.[42] We assume that the background salt of KCl is used to adjust the bulk concentration, yielding the following parameters used in the simulations: $\varepsilon_f = 7.08 \times 10^{-10}$ F/m, F = 96490 C/mol, T = 298 K, $\mu = 1 \times 10^{-3}$ Pa s, $D_1(K^+) = 1.957 \times 10^{-9}$ m^2/s, and $D_2(Cl^-) = 2.032 \times 10^{-9}$ m^2/s.[13]

In subsequent discussions, the bulk salt concentration in the right reservoir (C_R) is fixed at 1 mM and that in the left reservoir (C_L) ranges from 1 to 1000 mM. These asymmetric concentrations (e.g., $C_L > C_R$) establish a gradient across the nanopore and, therefore, both cations and anions are driven by diffusion from the high concentration reservoir toward the low concentration reservoir.

Figure 2a shows the $I-V$ curves for various levels of C_L/C_R, and reveals that the $I-V$ characteristics depend strongly on C_L/C_R. For $C_L/C_R = 1$, the electrolyte solution in the homogeneous

dx.doi.org/10.1021/ac4040136 | Anal. Chem. 2014, 86, 2681−2686

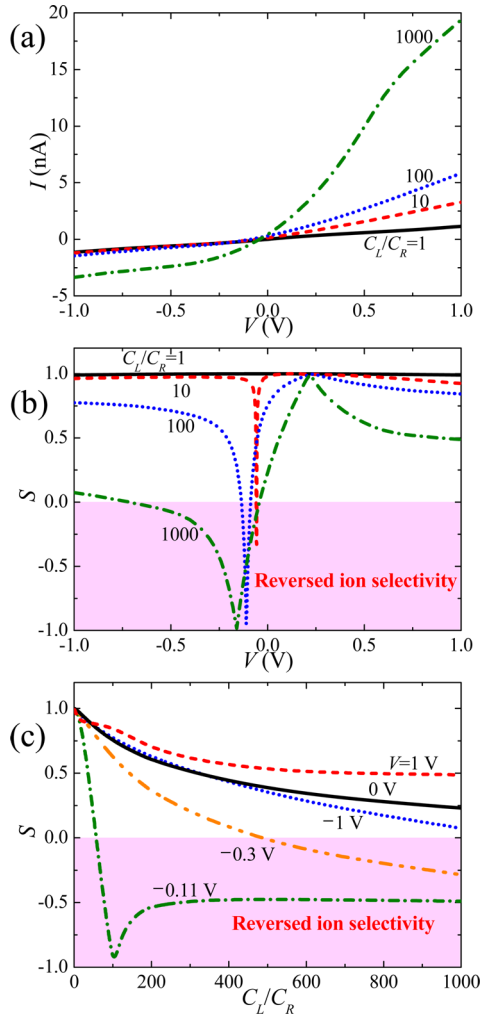

Figure 2. (a) Current I and (b) ion selectivity, S, of the nanopore vs the applied voltage, V, for various salt concentration ratios, C_L/C_R, and (c) S as a function of C_L/C_R for various values of V at C_R = 1 mM. The pink regions (S < 0) highlight where the ion selectivity of the nanopore is reversed.

nanopore behaves as an ohmic resistor, which is expected and consistent with the experimental observation.[39,41] If the value of C_L/C_R is relatively large, the current for positive V is larger than that for negative V, implying that a diodelike I–V behavior, referring to the ICR phenomenon, occurs. A similar phenomenon was also observed experimentally in five long silica nanochannels of 60 μm in length under a salt concentration gradient.[17] This rectification behavior can be attributed to the competitive effects of the applied electric field and concentration gradient across the nanopore, as schematically illustrated in Figure 1b. If the system is positively biased (e.g., V = +1 V), the directions of the applied electric field and salt gradient are the same, yielding enriched cations and anions within the nanopore and a larger ionic current. Otherwise, if the system is negatively biased (e.g., V = −1 V), the applied electric field is against the concentration gradient. In this case, the net driving force to ions is alleviated, resulting in a depletion of both cations and anions within the nanopore and a proportionally smaller current. These concentration-gradient-induced ion enrichment and depletion behaviors within the nanopore under different bias polarities can be illustrated by the cross-section-averaged ion conductivity, $\sigma = \sum_{j=1}^{2} \lambda_j c_j$, profiles shown in Figure 3. For simplicity, we assume that both the molar conductivity of K^+ ions (λ_1 = 7.352 × 10^{-3} S m^2 mol^{-1}) and

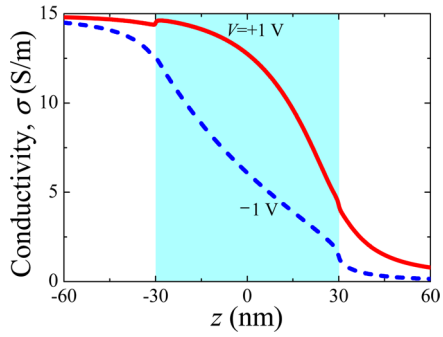

Figure 3. Axial variations of the cross-section-averaged ion conductivity σ over the nanopore radius for V = +1 V(solid line) and V = −1 V (dashed line) at C_L/C_R = 1000. The blue region (−30 nm ≤ z ≤ 30 nm) highlights the region of the nanopore.

that of Cl^- ions (λ_2 = 7.634 × 10^{-3} S m^2 mol^{-1}) are constant. Figure 3 clearly reveals that the ion conductivity within the nanopore (blue region) at +1 V is obviously higher than that at −1 V, in accordance with the ICR phenomenon. The efficiency of the ICR characteristics can be quantified by the current rectification factor, $R_f(|V|) = |I(+V)/I(-V)|$.[23,40] For example, R_f = 1 represents a nonrectifying, ohmic system (C_L/C_R = 1 in Figure 2a) and deviates from 1, denoting the diodelike systems (C_L/C_R > 1 in Figure 2a). In Figure 2a, $R_f(|V|$ = 1 V) increases with an increase in the level of C_L/C_R and is about 6 for C_L/C_R = 1000.

It is generally accepted that the ion selectivity of the nanopore highly depends on its charge properties.[9−12] For example, if the nanopore is negatively charged, the majority of transport ions are cations and, therefore, the nanopore displays cation-selective (i.e., the ionic current stemming from cations, $I_{counter}$, is larger than that from anions, I_{co}).[9−12] Figure 2 (panels b and c) depict the influences of the voltage and the concentration ratio on the ion selectivity of the nanopore, S. As shown in these two figures, in the absence of a concentration gradient (i.e., C_L/C_R = 1), the negatively charged nanopore, as expected, is nearly perfectly cation-selective ($S \approx 1$ and $I_{counter} \gg I_{co}$) due to the significant EDL overlapping inside it. In the presence of a concentration gradient (i.e., $C_L/C_R \neq 1$), the nanopore is still cation-selective ($0 < S \leq 1$ and $I_{counter} > I_{co}$) when the system is positively biased ($V > 0$) and the magnitude of the negative bias, $|V|$, is sufficiently small and large. However, the negatively charged nanopore becomes anion-selective ($-1 \leq S < 0$ in pink regions) when the magnitude of the negative bias, $|V|$, is moderately small. This implies that the ion selectivity of a negatively charged nanopore is reversed under appropriate conditions, thus apparently suggesting that the nanopore selectivity can be tuned from counterion- to co-ion-selective by adjusting the salt concentration gradient across it.

The nanopore ion selectivity behaviors seen in Figure 2 (panels b and c) can be explained by Figure 4, where the cross-section-averaged ionic fluxes of species j (solid curves for cations J_{N1} and dashed curves for anions J_{N2}) for four values of V in Figure 2c are plotted. These values are schematically represented in Figure 1b, which illustrates the following concept. If no potential bias is applied (V = 0), the concentration gradient, $-\nabla C$, imposed between the two reservoirs diffusively drives both cations and anions toward

dx.doi.org/10.1021/ac4040136 | Anal. Chem. 2014, 86, 2681−2686

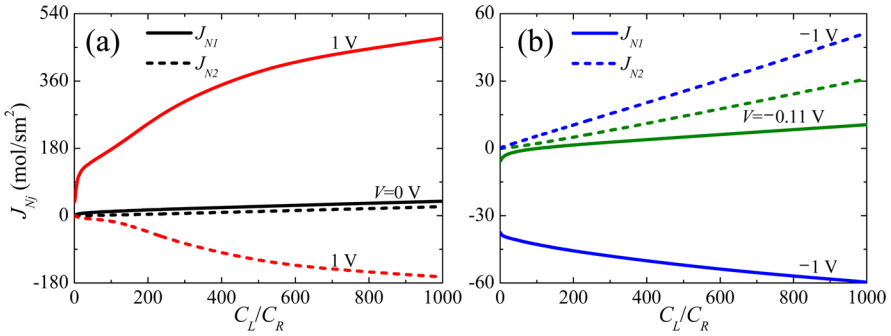

Figure 4. Cross-section-averaged ionic fluxes of species j (solid curves for cations J_{N1} and dashed lines for anions J_{N2}) in the nanopore as a function of C_L/C_R for the case of Figure 2c at (a) V = 0 and 1 V and (b) −0.11 and −1 V.

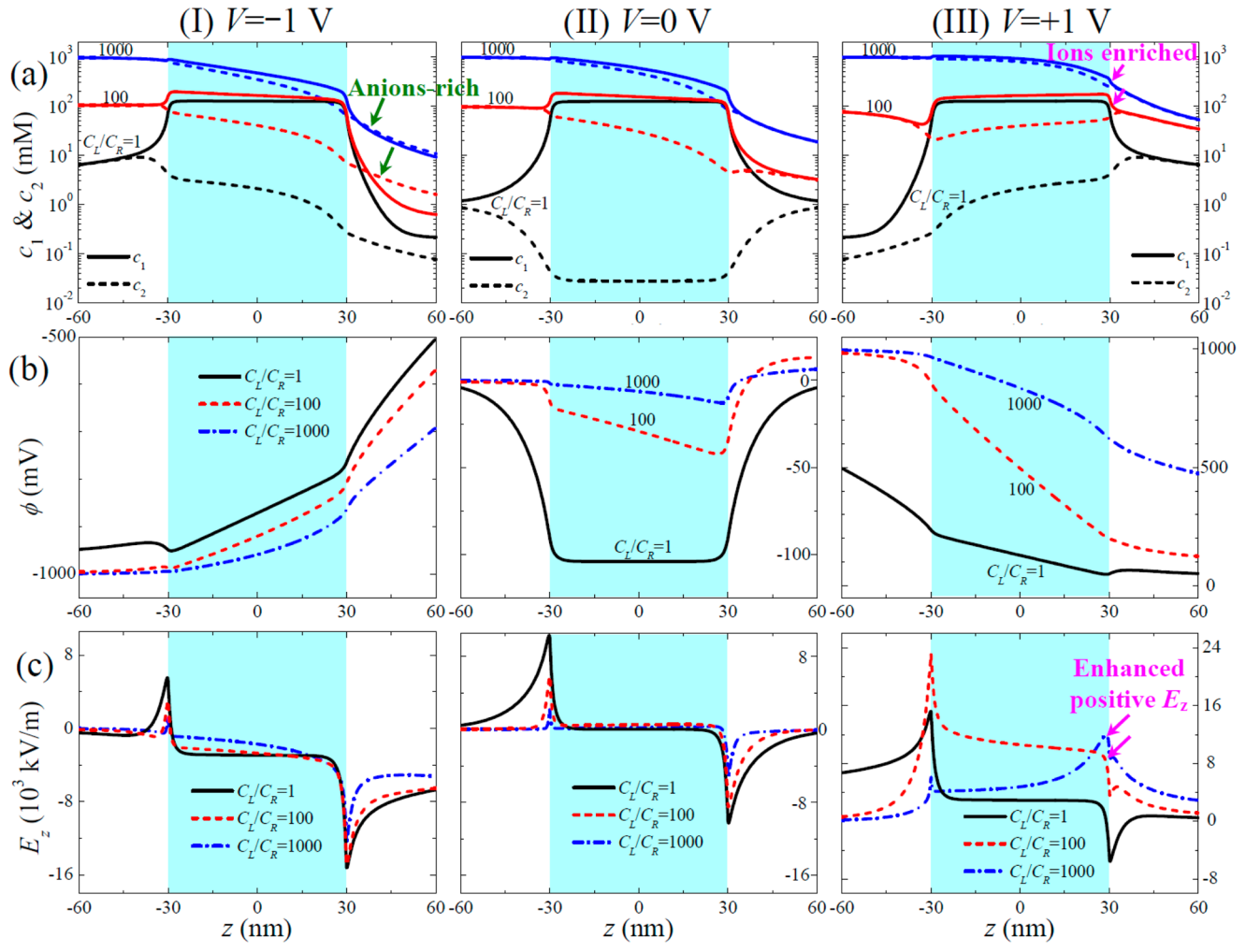

Figure 5. (a) Axial variations of the cross-section-averaged ionic concentrations (solid lines for cations c_1 and dashed lines for anions c_2), (b) electric potential, ϕ, and (c) axial electric field, $E_z = -\partial\phi/\partial z$, over the nanopore radius for various C_L/C_R at C_R = 1 mM. The first, second, and third columns represent the applied voltage V = −1, 0, 1 V, respectively. The blue regions (−30 nm ≤ z ≤ 30 nm) highlight the region of the nanopore.

the lower concentration side. In this case, both J_{N1} and J_{N2} are positive and J_{N1} is larger than J_{N2} due to the EDL overlapping, as shown in Figure 4a. Moreover, if a positive (negative) bias is applied in the left reservoir, a positive (negative) electric field is induced, driving cations toward the right (left) side of the nanopore and anions toward the left (right) side of the nanopore. As a result, for a positive bias (e.g., +1 V), the directions of the concentration gradient, $-\nabla C$, and the electric field, $-\nabla V$, are identical (Figure 1b), leading to a strong driving force to prompt cations toward the right reservoir. In this case, J_{N1} is significantly larger than $|J_{N2}|$ and, therefore, the nanopore is cation-selective, as shown in Figure 4a. On the other hand, if the negative bias is sufficiently large (e.g., −1 V), the applied electric field, $-\nabla V$, is against the imposed concentration gradient, $-\nabla C$. Because the magnitude of the former is significantly higher than that of the latter, the nanopore is still cation-selective ($|J_{N1}| > J_{N2}$), as can be seen in Figure 4b. It is worth noting in Figure 4b that if the negative bias is moderately

dx.doi.org/10.1021/ac4040136 | Anal. Chem. 2014, 86, 2681−2686

weak (e.g., −0.11 V), J_{N1} turns from negative into positive when the concentration gradient across the nanopore is sufficiently large. In this case, the ionic flux of cations migrates in the same direction as that of anions. The magnitude of the former is smaller than that of the latter, implying that the nanopore becomes anion selective (Figure 1b). Apparently, the ion selectivity of a charged nanopore can be actively modulated by the applied concentration gradient and potential bias.

To further elaborate the influences of the applied concentration gradient and potential bias on the ion transport phenomena in the nanopore, Figure 5 depicts the axial variations of the cross-section-averaged ionic concentrations, electric potential, and axial electric field, $E_z = -\partial\phi/\partial z$, over the nanopore radius. Since the nanopore is negatively charged, more counterions (cations) are attracted into the nanopore, while co-ions (anions) are expelled out. The concentration of cations (solid lines) becomes much higher than that of co-ions (dashed lines) within the nanopore (blue regions), regardless of the levels of the applied concentration gradient and the potential bias (Figure 5a). Therefore, the magnitude of the cation (anion) flux inside the nanopore is significantly larger (smaller) than that in the reservoirs, as schematically depicted in Figure 1a. This results in two ICP phenomena compared to the case for $V = 0$ V (Figure 5a, II): (i) ions are enriched (depleted) near the left (right) opening of the nanopore if $V = -1$ V (Figure 5a, I) and (ii) a reversed trend is observed for $V = +1$ V (Figure 5a, III).

It is worth noting in Figure 5a, II that if a higher (lower) salt concentration is applied on the left (right) reservoir, the EDL near the left (right) part of the nanopore is thinner (thicker), as schematically illustrated in Figure 1a. Both cations and anions are, therefore, able to migrate into the left part of the nanopore, suggesting that anions do not accumulate there, which contradicts the conclusions made by Liu et al.[43] and Lo et al.[44] On the other hand, because EDL overlapping near the right part of the nanopore is more significant, cations (anions) are accumulated (expelled), making it easier (harder) for cations (anions) to migrate through the entire nanopore. As a result, if $V = +1$ V is applied (Figure 5a, III), ions are significantly enriched near the right opening of the nanopore compared to the case of $V = 0$ V, leading to the EDL there becoming thinner, especially in the presence of the concentration gradient. This amplified effect occurring when $C_L/C_R > 1$ results in a smooth and decreasing electric potential profile near the right opening of the nanopore (Figure 5b, III) and, therefore, a remarkably enhanced positive electric field (Figure 5c, III). Note that the direction of the electric field (positive) for $C_L/C_R > 1$ is distinctly different from that for $C_L/C_R = 1$ (negative). The former is favorable to enhance the capture rate of negatively charged nanoparticles from the right reservoir into the nanopore, but the latter reduces the capture rate. A similar concept was adopted by Wanunu et al.,[45] who experimentally demonstrated that applying a concentration gradient in the same direction of the electric field across a silicon nitride nanopore was capable of enhancing the DNA capture rate. They, however, attributed this important finding to the selective pumping of cations (K^+) from the high to low concentration sides of the nanopore, thereby inducing a cations-rich electrostatic field to capture negatively charged DNA. In fact, the concentration of cations is substantially higher than that of anions in the negatively charged nanopore regardless of the presence and absence of a salt gradient (Figure 5a). As demonstrated in Figure 5c, III, the enhanced DNA capture rate should result from the reversed amplified positive electric field occurring near the cathode side of the nanopore in the presence of the applied concentration gradient.

On the contrary, if $V = -1$ V is applied (Figure 5a, I), ions are slightly enriched near the left opening of the nanopore in the presence of the applied concentration gradient (e.g., $C_L/C_R = 100$ and 1000) compared to the case of $V = 0$ V. This is because the magnitude of the ionic flux of cations (anions) in the nanopore is slightly larger (smaller) than that of cations (anions) in the left reservoir because of a less significant EDL overlapping at higher salt concentration there. This slight enrichment of ions for $C_L/C_R = 100$ and 1000 induces an electric field, the direction of which is opposite to that of the applied one, yielding a lower net electric field in the left opening of the nanopore (Figure 5c, I), which decreases the capture rate of negatively charged biomolecules from the left reservoir into the nanopore. It is interesting to note in Figure 5a, I that a surprising anions-rich phenomenon occurs outside the right opening of the nanopore in the presence of the applied concentration gradient. This phenomenon can be attributed to the significant EDL overlapping near the right part of the nanopore, resulting in more anions expelled from the nanopore into the right reservoir. This anions-rich phenomenon might induce a negative electrostatic field to prevent the DNA translocation through the nanopore, which explains why the DNA translocation events in nanopore sensing experiments are significantly reduced when the applied concentration gradient is against the applied electric field.[45]

CONCLUSIONS

In summary, we have theoretically demonstrated that an applied concentration gradient can be utilized to regulate the ion transport and selectivity in a charged nanopore. The diodelike current−voltage characteristics is found in the presence of the concentration gradient. The ion selectivity of a charged nanopore is reversed from counterion-selective to co-ion-selective if the concentration gradient is sufficiently large. Moreover, we also show that a reversed amplified local electric field occurs near the cathodic side of the nanopore, if the directions of the applied electric field and concentration gradient are the same. This unique reversed electric field can be applied to enhance the capture rate of negatively charged (bio)nanoparticles from the cathode reservoir into a negatively charged nanopore and clearly explains why the DNA capture rate is significantly enhanced in the nanopore sensing experiment.[45] The results demonstrate that one can regulate ion and (bio)nanoparticle transport in a charged nanopore by simultaneously tuning the applied electric field and salt concentration gradient.

AUTHOR INFORMATION

Corresponding Authors

*E-mail: lhyeh@yuntech.edu.tw. Fax: +886-5-5312071.

*E-mail: sqian@odu.edu.

Author Contributions

‖L.-H.Y. and C.H. contributed equally to this work.

Notes

The authors declare no competing financial interest.

ACKNOWLEDGMENTS

This work was supported by the National Science Council of the Republic of China (Grants NSC-102-2221-E-224-052-MY3

and NSC-103-2218-E-002-010) (L.H.Y.), the State Scholarship Fund of China under Grant 2011684502 (Z.Z.), and NSF DUE-0940895 (S.Q.).

REFERENCES

(1) Dekker, C. *Nat. Nanotechnol.* **2007**, *2*, 209−215.
(2) Howorka, S.; Siwy, Z. *Chem. Soc. Rev.* **2009**, *38*, 2360−2384.
(3) Venkatesan, B. M.; Bashir, R. *Nat. Nanotechnol.* **2011**, *6*, 615−624.
(4) Haque, F.; Li, J. H.; Wu, H. C.; Liang, X. J.; Guo, P. X. *Nano Today* **2013**, *8*, 56−74.
(5) Hou, X.; Guo, W.; Jiang, L. *Chem. Soc. Rev.* **2011**, *40*, 2385−2401.
(6) Guan, W. J.; Reed, M. A. *Nano Lett.* **2012**, *12*, 6441−6447.
(7) Guo, W.; Tian, Y.; Jiang, L. *Acc. Chem. Res.* **2013**, *46*, 2834−2846.
(8) Cervera, J.; Alcaraz, A.; Schiedt, B.; Neumann, R.; Ramirez, P. *J. Phys. Chem. C* **2007**, *111*, 12265−12273.
(9) Cervera, J.; Schiedt, B.; Neumann, R.; Mafe, S.; Ramirez, P. *J. Chem. Phys.* **2006**, *124*, 104706.
(10) Vlassiouk, I.; Smirnov, S.; Siwy, Z. *Nano Lett.* **2008**, *8*, 1978−1985.
(11) Yeh, L. H.; Zhang, M.; Qian, S. *Anal. Chem.* **2013**, *85*, 7527−7534.
(12) Schoch, R. B.; Han, J. Y.; Renaud, P. *Rev. Mod. Phys.* **2008**, *80*, 839−883.
(13) Yeh, L. H.; Zhang, M.; Hu, N.; Joo, S. W.; Qian, S.; Hsu, J. P. *Nanoscale* **2012**, *4*, 5169−5177.
(14) Kim, S. J.; Li, L. D.; Han, J. *Langmuir* **2009**, *25*, 7759−7765.
(15) Yeh, L. H.; Zhang, M.; Qian, S.; Hsu, J. P.; Tseng, S. *J. Phys. Chem. C* **2012**, *116*, 8672−8677.
(16) Siwy, Z. S. *Adv. Funct. Mater.* **2006**, *16*, 735−746.
(17) Cheng, L. J.; Guo, L. J. *Nano Lett.* **2007**, *7*, 3165−3171.
(18) Karnik, R.; Duan, C. H.; Castelino, K.; Daiguji, H.; Majumdar, A. *Nano Lett.* **2007**, *7*, 547−551.
(19) Ali, M.; Ramirez, P.; Mafe, S.; Neumann, R.; Ensinger, W. *ACS Nano* **2009**, *3*, 603−608.
(20) Lan, W. J.; Holden, D. A.; White, H. S. *J. Am. Chem. Soc.* **2011**, *133*, 13300−13303.
(21) Cao, L. X.; Guo, W.; Wang, Y. G.; Jiang, L. *Langmuir* **2012**, *28*, 2194−2199.
(22) Liu, J.; Wang, D.; Kvetny, M.; Brown, W.; Li, Y.; Wang, G. *Anal. Chem.* **2012**, *84*, 6926−6929.
(23) Tagliazucchi, M.; Rabin, Y.; Szleifer, I. *ACS Nano* **2013**, *7*, 9085−9097.
(24) Cheng, L. J.; Guo, L. J. *Chem. Soc. Rev.* **2010**, *39*, 923−938.
(25) He, Y.; Gillespie, D.; Boda, D.; Vlassiouk, I.; Eisenberg, R. S.; Siwy, Z. S. *J. Am. Chem. Soc.* **2009**, *131*, 5194−5202.
(26) Maffeo, C.; Bhattacharya, S.; Yoo, J.; Wells, D.; Aksimentiev, A. *Chem. Rev.* **2012**, *112*, 6250−6284.
(27) Daiguji, H.; Yang, P. D.; Majumdar, A. *Nano Lett.* **2004**, *4*, 137−142.
(28) Yeh, L. H.; Zhang, M.; Qian, S.; Hsu, J. P. *Nanoscale* **2012**, *4*, 2685−2693.
(29) He, Y. H.; Tsutsui, M.; Fan, C.; Taniguchi, M.; Kawai, T. *ACS Nano* **2011**, *5*, 5509−5518.
(30) van Dorp, S.; Keyser, U. F.; Dekker, N. H.; Dekker, C.; Lemay, S. G. *Nat. Phys.* **2009**, *5*, 347−351.
(31) Lan, W. J.; Holden, D. A.; Zhang, B.; White, H. S. *Anal. Chem.* **2011**, *83*, 3840−3847.
(32) Lan, W. J.; White, H. S. *ACS Nano* **2012**, *6*, 1757−1765.
(33) Corry, B.; Kuyucak, S.; Chung, S. H. *Biophys. J.* **2000**, *78*, 2364−2381.
(34) Yeh, L. H.; Xue, S.; Joo, S. W.; Qian, S.; Hsu, J. P. *J. Phys. Chem. C* **2012**, *116*, 4209−4216.
(35) Kubeil, C.; Bund, A. *J. Phys. Chem. C* **2011**, *115*, 7866−7873.
(36) Yeh, L. H.; Zhang, M. K.; Joo, S. W.; Qian, S.; Hsu, J. P. *Anal. Chem.* **2012**, *84*, 9615−9622.
(37) He, Y. H.; Tsutsui, M.; Fan, C.; Taniguchi, M.; Kawai, T. *ACS Nano* **2011**, *5*, 8391−8397.
(38) He, Y. H.; Tsutsui, M.; Scheicher, R. H.; Bai, F.; Taniguchi, M.; Kawai, T. *ACS Nano* **2013**, *7*, 538−546.
(39) Smeets, R. M. M.; Keyser, U. F.; Krapf, D.; Wu, M. Y.; Dekker, N. H.; Dekker, C. *Nano Lett.* **2006**, *6*, 89−95.
(40) Ai, Y.; Zhang, M. K.; Joo, S. W.; Cheney, M. A.; Qian, S. *J. Phys. Chem. C* **2010**, *114*, 3883−3890.
(41) Chang, H.; Kosari, F.; Andreadakis, G.; Alam, M. A.; Vasmatzis, G.; Bashir, R. *Nano Lett.* **2004**, *4*, 1551−1556.
(42) Stein, D.; Kruithof, M.; Dekker, C. *Phys. Rev. Lett.* **2004**, *93*, 035901.
(43) Liu, K. L.; Hsu, J. P.; Tseng, S. *Langmuir* **2013**, *29*, 9598−9603.
(44) Lo, T. W.; Hsu, C.; Liu, K. L.; Hsu, J. P.; Tseng, S. *J. Phys. Chem. C* **2013**, *117*, 19226−19233.
(45) Wanunu, M.; Morrison, W.; Rabin, Y.; Grosberg, A. Y.; Meller, A. *Nat. Nanotechnol.* **2010**, *5*, 160−165.